JMEPEG (2012) 21:231–239
DOI: 10.1007/s11665-011-9894-3

1059-9495/$19.00

The Comparative Effect of Sugarcane Juice on the Abrasion-Corrosion Behavior of Fe-Cr-B Electric Arc Sprayed and Fe-Cr-C Weld Coatings

Vernon E. Buchanan

(Submitted July 21, 2010; in revised form December 28, 2010)

Abrasion-corrosion tests were conducted on two commonly Fe-Cr-C shielded metal arc welding (SMAW) hardfacings used in the sugar industry and an arc sprayed Fe-Cr-based coating. The tests were performed on a modified block-on-ring tester with the coatings sliding against compressed sugarcane fiber in the presence of abrasive slurry. The findings showed that, in the presence of sugarcane juice and sand slurry, the SMAW coatings had similar wear performance while the abrasive wear of the arc-sprayed coating was superior to the SMAW coatings. In the presence of a neutral solution, the material loss from the arc-sprayed coating was similar to that obtained in the sugarcane juice while the SMAW coatings showed a marked decrease; this demonstrated that the arc-sprayed coating was more desirable in an abrasive-corrosion environment. The study also showed that the resistance to material does not follow the expected trend, in which wear resistance increases with increasing hardness.

Keywords arc spraying, corrosion, hardfacing, microstructure, welding

1. Introduction

The need to increase production rate and to keep up with rapid technological advances have pushed metallurgists to develop new materials that have longer working life and higher wear resistance. In this context, the need to increase the extraction rate of sucrose from sugarcane has led to increase pressures on the sugarcane mill roller and, consequently, the need for improved surfacing of the sugarcane rollers with better abrasion-corrosion resisting materials.

The sugarcane mill roller is comprised essentially of a forged steel shaft onto which a gray cast iron shell is shrunken. The circumference of the shell is machined with a series of V-shaped grooves, evenly spaced along its length. Thus, a longitudinal section gives a serrated tooth outline. Current methods to improve wear resistance of the cast iron shell include the deposition of Fe-Cr-C alloy (Ref 1, 2) or WC particles in a metal matrix (Ref 3) around the upper section of the roller teeth. These methods have reported significant reduction in the frequency to re-hardfaced the teeth. The Fe-Cr-C alloys are most commonly used, the presence of chromium provides corrosion resistance and the hard chromium carbide precipitates increase resistance to abrasion.

Although the coatings deposited on the rollers have been developed to specifically suit the welding procedures and environment in the mill, the expected properties of the coatings are frequently not achieved. Several factors determine the efficiency of the weld, which include the type and size of electrode, the welding process, the deposit rate, and the electrical parameters (Ref 4). High Fe-Cr-C weld deposits are also prone to cracking and spallation due to the difference in thermal expansion with gray cast iron (Ref 5). Cracks are often produced within the iron phosphide eutectic regions in the heat-affected zone of the gray cast iron substrate, which precipitates the removal of large pieces of tooth. In addition, French and Klanjscek (Ref 6) have shown that the expected microstructure was not achieved in some of the weld deposits but consisted of a hypoeutectic Fe-Cr-C alloy from almost all austenite to about 70% eutectic.

Thermal spraying process has been used to produce high Fe-Cr-based alloys that exhibited comparable hardness (Ref 7-9) and wear resistance (Ref 9) than as-cast alloys of similar composition. In light of its deposit efficiency, cost effectiveness and the ability to produce thick coatings (Ref 10), the electric arc spraying process is seen an alternative to the hardfacings of roller shells with shielded metal arc welding (SMAW). Thus, this study will investigate the comparative abrasion-corrosion behavior of an arc-sprayed coating with commonly used SMAW coatings.

2. Experimental Procedure

2.1 Materials and Deposition of Coatings

The base material for the overlay coatings was gray cast iron; the chemical analysis is shown in Table 1. Two commercially available SMAW hardfacing electrodes, commonly used in the sugar industry, were used to deposit the welds. Their chemical compositions are shown in Table 2. The electric arc-sprayed material was a Fe-Cr-B wire of 1.6-mm diameter and of chemical composition Fe-26Cr-3B-1Mn-0.3C wt.%.

Vernon E. Buchanan, University of Technology, Jamaica, 237 Old Hope Road, Kingston 6, Jamaica, West Indies. Contact e-mail: vbuchanan@utech.edu.jm.

Table 1 Chemical composition (wt.%) of gray cast iron disc

C	Si	Mn	P	S	Ni	Cr	Mo	Cu	Fe
3.64	1.90	0.66	0.09	0.13	0.08	0.14	0.03	0.02	Bal

Table 2 Chemical composition (wt.%) of SMAW electrodes

	W1		W2	
	Metallic wire	Flux coating	Metallic wire	Flux coating
C	···	10.42	···	9.78
Si	<0.01	1.82	<0.01	2.21
S	0.04	<0.01	0.05	<0.01
Mn	0.47	3.12	0.41	3.71
Cr	0.04	29.48	0.01	29.12
P	<0.01	<0.01	<0.01	<0.01
Ni	<0.01	<0.01	<0.01	<0.01
Mo	<0.01	<0.01	<0.01	<0.01
Cu	···	<0.01	···	<0.01
Al	···	1.07	···	2.25
Ca		2.23		1.58
Mg	···	1.17	···	1.33
Ti				4.43
Fe	Balance		Balance	

Experimental details of the deposition of the coatings were described elsewhere (Ref 10). In summary, two SMAW hardfaced coatings, designated W1 and W2, and one arc-sprayed coating, designated S1, were deposited onto a 90 mm diameter × 20 mm wide gray cast iron discs. After grinding the circumference of the coated discs to approximately R_a=6 μm, the final diameter of the disc was 100 mm.

2.2 Microstructural, Chemical, and Quantitative Analysis

Coated samples were also prepared for optical examination by conventional grinding, polishing, and etching. The SMAW and arc-sprayed coatings were etched in Vilella's (one part HNO_3, two parts HCl, and three parts glycerol) and Murakami's (3 g $K_3Fe(CN)_6$ + 10 g NaOH + 100 mL H_2O) reagent, respectively. The worn surfaces and immediate subsurfaces were examined with a Phillips XL30 field emission gun scanning electron microscope (SEM), using both secondary electrons (SE) and backscattered electrons (BSE). The carbides present in the SMAW coatings were identified by x-ray diffraction (XRD), using Cu K_α radiation. The samples were scanned from $2\theta = 15°$ to 140° with a step size of 0.02°.

A PC-based image analysis software was used to quantitatively analyze the microstructures, which include porosity, carbide size, carbide volume, and splat thickness. The microhardness of the upper section of the coatings was measured with a Vickers microhardness tester at a load of 300 gf for 15 s, after polishing the surfaces with an 800-grit paper. The SMAW specimens were then etched and additional microhardness measurements, using a load of 100 gf, were conducted on the primary carbides located in the upper layers of the weld.

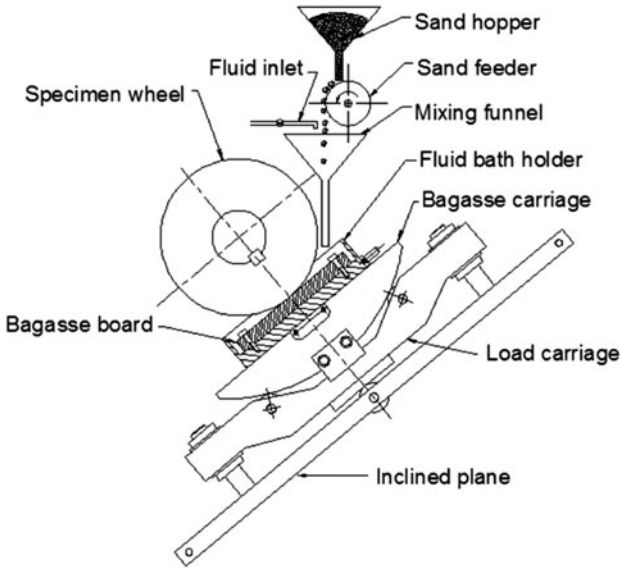

Fig. 1 Schematic arrangement of the multistation block-on-ring wear test machine showing location of specimen wheel, bagasse board, and method of feeding the slurry

2.3 Abrasive Test and Data Collection

The wear test was evaluated using a modified multistation block-on-ring machine, which was presented elsewhere (Ref 10). In summary, bagasse board (compressed bagasse) was placed in the fluid bath holder and the coated discs replaced the rubber wheel. The arrangement, shown in Fig. 1, was inclined at 40° to the horizontal to allow the abrasive slurry to pass over the bagasse board, which was contained between two side plates so that the abrasives were constrained to pass through the wear zone. The slurries used were a mixture of (1) silica sand and sugarcane juice (pH 4.5) and (2) silica sand and glycerol. The sand was sieved into a particle size range 211-300 μm, and the average microhardness (HV) of the sand was ~800 kgf/mm^2 at a load of 300 gf.

Water was added to glycerol to match the viscosity of the sugarcane juice.

Prior to testing, the specimens were washed with soap and water, rinsed in acetone, dried and then weighed. Loads ranging from 80 to 150 N were applied. The speed was kept constant at 100 rpm giving a surface speed of 524 mm/s, which approached the maximum value in most sugarcane mill roller setting. The sand was placed into a hopper and fed at a constant rate (22 ± 4 g/min) into the wear zone by means of a sand feeder composed of a rotating plastic drum with a shallow groove driven by a variable speed motor. The abrasive slurry was formed by adding sugarcane juice (pH 4.5) to the metered sand in a mixing funnel just before the abrasive entered the wear zone. The rate of flow of the aqueous medium, nominally 50 mL/min, was occasionally adjusted to ensure that the slurry was sufficiently mobile to pass through the funnel and also to ensure that the slurry did not rise too high above the wear zone. The test was carried out once on each set of conditions by making the test run sufficiently long to minimize error. The sliding distance was confirmed by repeating a test with a cast iron disc at loads of 80, 120, and 150 N in the slurry condition (sugarcane juice + abrasive) and which a maximum difference of 15% in mass loss was recorded.

A fresh bagasse board and re-ground disc were used for each set of tests. The laboratory test was carried out within the air temperature range 24-27 °C and relative humidity of 40-60%.

Weight loss was determined using a Satorius CP2202S electronic balance, which had a resolution of 0.01 g. Each test was run for 4 h, which was equivalent to a sliding distance of 7500 m. At intervals of 1 h the disc was removed, washed, rinsed in acetone, dried, and weighed.

3. Results

3.1 Microstructure

Figures 2 and 3 show the XRD pattern and the optical micrographs of the SMAW coatings, respectively, used in the test. The coatings, W1 and W2, are composed of primary M_7C_3 carbides in a matrix of essentially ($\gamma + M_7C_3$), the "M" mainly representing the metallic species Fe and Cr. Although both SMAW coatings had approximately the same total carbide volume fraction (CVF) of approximately 59%, the estimated CVF of the primary carbides in W1 and W2 were 26 and 35%, respectively. Quantitative measurement by point counting showed that the number of the primary carbide particles per mm^3 averaged 500 and 241 for W1 and W2, respectively, which meant that the average size of the primary carbides in W2 was significantly larger than those in W1. This was also evident by visual examination.

Figure 3(c) is the micrograph of the arc-sprayed coating in which the characteristic splat structure can be clearly seen. In addition to the metallic matrix, the figure shows dark oxide inclusions and porosity, the volume fraction of each being 4.5 and 2%, respectively. The average splat thickness was determined from 39 fields, each 175 × 110 μm, using the linear intercept method (Ref 11). The splat thickness varied from 2 to 91 μm with an average thickness of 10 μm/field and a standard deviation of 1.5 μm.

The microhardness of the coatings and primary carbides are shown in Table 3. Statistically, there is no difference in hardness between W1 and W2, while S1 has a lower hardness value.

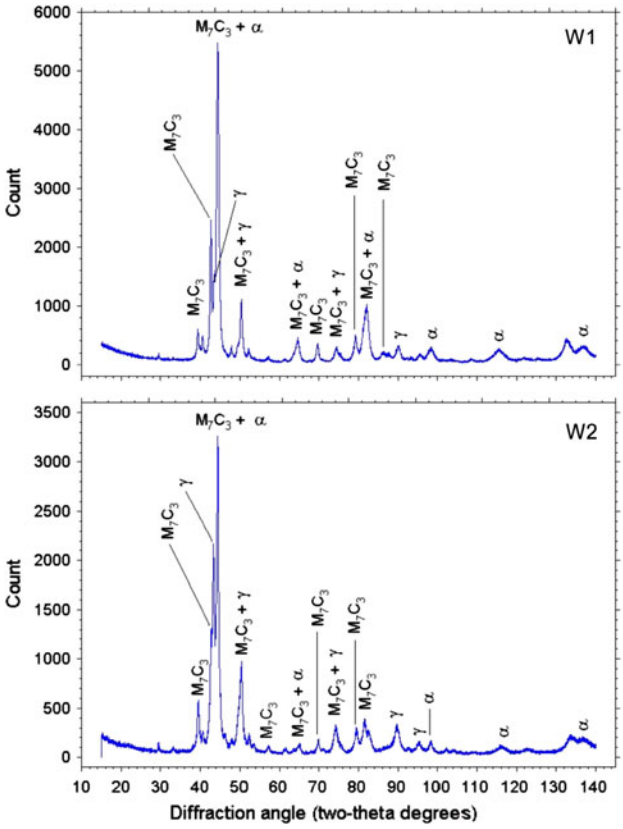

Fig. 2 XRD patterns of SMAW coatings W1 (top) and W2 (bottom)

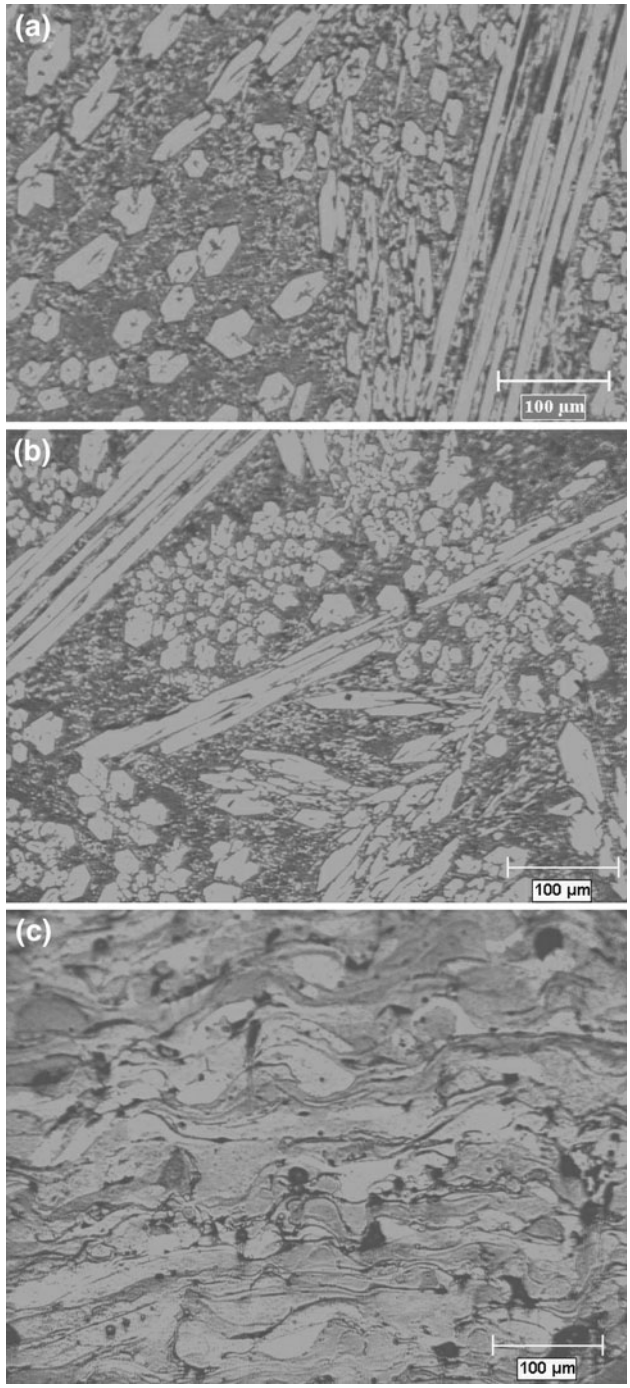

Fig. 3 Optical micrographs of the cross sections of coatings showing typical features of (a) W1, (b) W2, and (c) S1

3.2 Wear in Slurries

Figure 4 shows the plot of mass losses of the coatings against sliding distance at different loads in the sugarcane juice slurry. Overall, the wear of the SMAW coatings was a least twice that experienced by the arc-sprayed coating. In all cases, the law (Ref 12)

$$V = \frac{K_{abr} L x}{H}, \quad \text{(Eq 1)}$$

where V is the wear volume, K_{abr} is a proportionality constant, L is the load, x is the distance, and H is the hardness of the material being abraded, was supported as the wear loss almost increased linearly with sliding distance. By visual observation of Fig. 4, steady-state wear was assumed to start from 1872 m. The effect of load on the wear of the coatings at steady state is plotted in Fig. 5, which demonstrates the proportionality of the loads investigated with wear loss. The arc-sprayed coating, S1, although being the softest, exhibits the lowest mass loss at all loads, while W2, although softer than W1, appears to be marginally better in wear resistance than W1 at the higher loads. The lower wear performance of the harder SMAW coating supports the findings of Chatterjee and Pal (Ref 13) for abrasive test conducted on similar hard-faced microstructures in which the mass loss results showed no correlation to the microhardness.

To further analyze the mass loss of the coatings, the data shown in Fig. 5 can be presented in the simplified form of Eq 1:

$$Q = kW \quad \text{(Eq 2)}$$

where Q is the wear rate (g/m), k is the wear coefficient (g/Nm), and W is the applied load (N). Figure 6 shows the steady-state wear coefficient of the coatings as a function of load. All coatings display slight transitional wear behavior at 120 N. W2 exhibits slightly better wear coefficient than W1

Table 3 Average microhardness (kgf/mm^2) of coatings, the "±" represents one standard deviation of the sample average

Coating	Microhardness of coating ($HV_{300\ gf}$)	Microhardness of primary carbides ($HV_{100\ gf}$)
W1	824 ± 75	1235 ± 122
W2	787 ± 91	1249 ± 71
S1	692 ± 110	NA

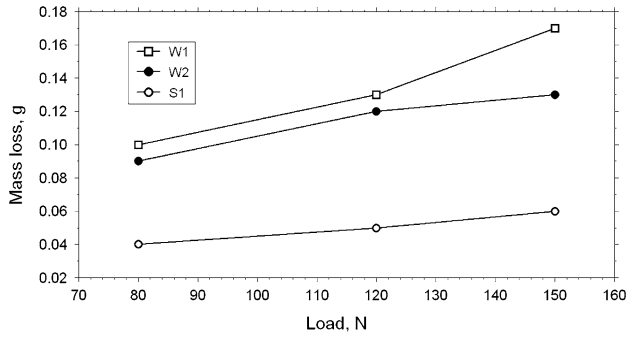

Fig. 5 Steady state mass loss of coatings in sugarcane juice slurry as a function of applied load

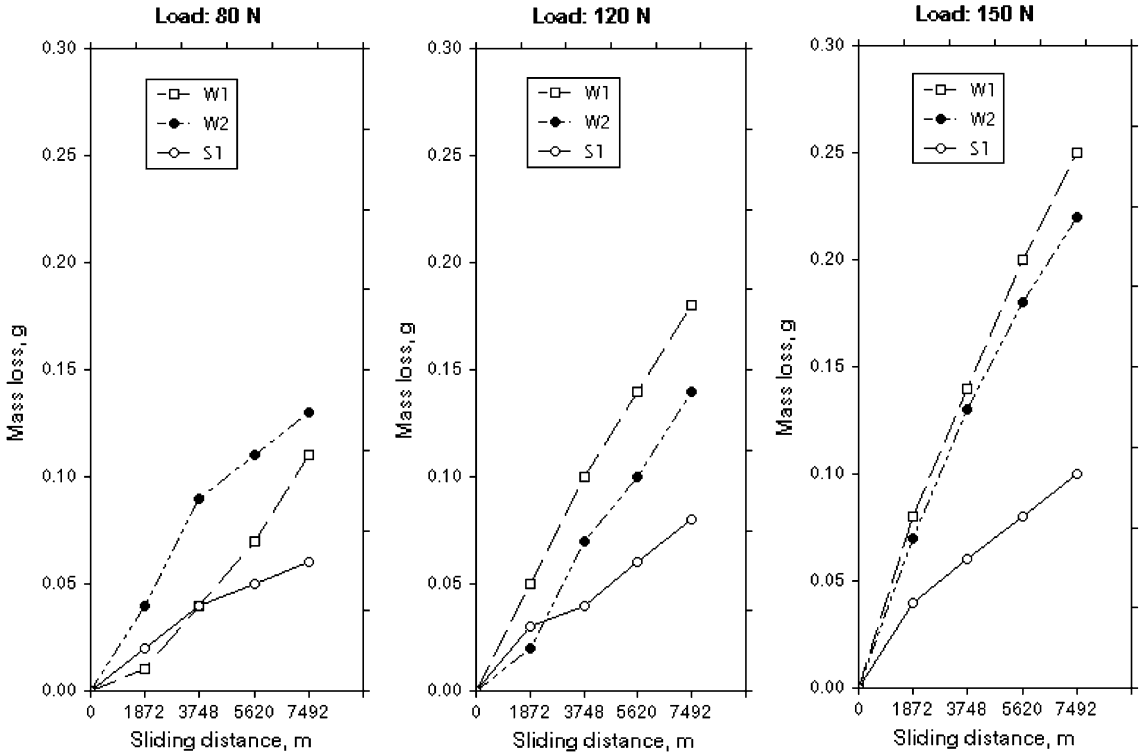

Fig. 4 Plots of mass loss versus sliding distance for the overlay coatings W1, W2, and S1 at different loads in slurry conditions (sugarcane juice and sand)

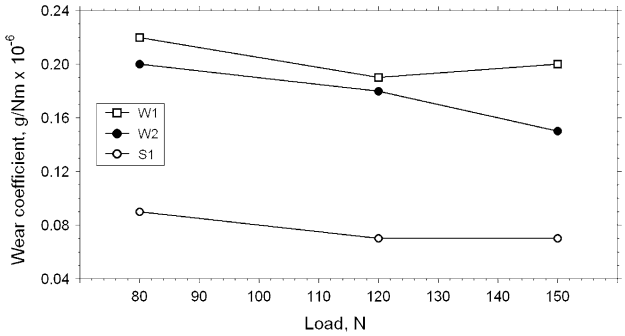

Fig. 6 Wear coefficient of coatings in sugarcane juice slurry at loads of 80, 120, and 150 N

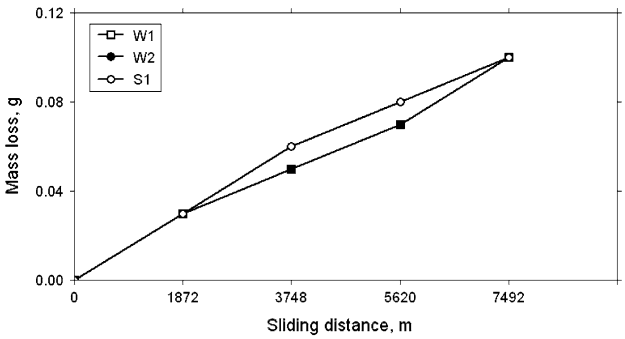

Fig. 7 Plots of mass loss versus sliding distance of coatings in glycerol slurry at a load of 150 N. Note that the plots of W1 and W2 coincide

and this can be attributed to its larger size primary carbides. It can also be seen that the wear coefficient of S1 is much less than those of W1 and W2.

To determine the effect of corrosion, the sugarcane juice was replaced with glycerol and the resulting mass losses at 150 N are presented in Fig. 7. The arc-sprayed coating has similar mass loss when compared with the test in sugarcane juice slurry; however, the SMAW coatings show significant reduction when compared with the sugarcane juice slurry. In addition, the steady-state mass loss in W1 and W2 coatings was reduced by 59 and 53%, respectively, whereas in S1, there was a 10% increase. The results demonstrate the superior wear resistance of the arc-sprayed coating in a corrosive medium.

3.3 Analysis of Worn Surfaces

Figure 8(a) and (b) show typical SEM images of the worn surfaces of the SMAW coatings generated during sliding against bagasse board in the sugarcane juice slurry. Shallow, intermittent grooves, running parallel to the sliding direction of the discs, were evident. Apparently, the abrasive particles were able to form grooves effectively through the matrix of the SMAW coatings but the grooves either stopped or became very shallow whenever primary carbides were in the path of the abrasives. This supports the underlying reason for using hypereutectic Fe-Cr-C alloys that primary chromium carbides are better able to resist abrasive wear than an austenitic/ferritic matrix.

Numerous craters were also visible in the images of the SMAW coatings, and a close study of the images indicated fewer craters in W2, which might explain the lower wear rate. The BSE images in Fig. 8(c, d) reveal that the craters were largely associated with carbide removal. In addition, the primary carbides have been fractured in several places with the resultant loss of material. There is also evidence of microgrooving in the primary carbides, such as in Fig. 8(c) that was probably caused from M_7C_3 debris trapped in the bagasse board.

In contrast to the SMAW coatings, the grooves in the arc-sprayed coating, Fig. 9(a), are generally longer, closer, and parallel to each other. While it appeared that carbide fracture was the dominant mode of material removal from the SMAW coatings, a microploughing-deformation mechanism could be considered as the dominant mode of material removal for the arc-sprayed coating. Closer examination of a grooved section of Fig. 9(a) that is encircled by the rectangle shows microcracks emanating within the grooves. The majority of cracks are believed to initiate at the splat boundaries and the remainder at the boundaries of oxides and inclusions.

Cross sections of the worn surfaces of the coatings were taken to investigate the extent of subsurface damages and to better understand the mechanism of wear. Figure 10 shows a longitudinal cross section of the coatings at 150 N in the presence of sand and sugarcane juice. In the SMAW coatings, Fig. 10(a, b), the cracks in the primary carbides have extended to ~50 μm into the coating. Figure 10(b) shows the initial stages of carbide removal, where the upper section of the large primary carbides have been severely broken into several pieces and are either being held together by the eutectic or the cracks have not propagated sufficiently in the direction perpendicular to the field of view to become detached. On the other hand, a section of Fig. 10(a) (marked "X") has been completely removed. The origin of crack initiation can be attributed to initial microcracks in the carbide during the solidification process. It has also been reported that cleavage of the weakly bonded carbide planes perpendicular to the *c*-axis under shear stresses can result in loss of carbide (Ref 14).

It is evident from the appearance of the subsurface zone of the arc-sprayed coating that material removal occurred not only through ploughing and cutting, but also by virtue of separation of the top layers (splats) from the surface. Figure 10(c) shows a particle that was about to be removed. The particle, composed of several splats, appears to fracture at the weakest bond, probably due to the occurrence of the thin oxide or porous layer between the splats.

The microhardness of S1 at approximately 25 μm beneath the worn surface was measured with a 100 gf load, and the average value was 782 kgf/mm^2 with a standard deviation of 114 kgf/mm^2. This is harder than the unworn coating (Table 3) and indicates that plastic strain hardening had occurred.

4. Discussion

The abrasive wear of the coatings in the slurries was generally proportional to the load; however, the arc-sprayed coating exhibited superior wear resistance in comparison with the SMAW coatings, which displayed similar wear characteristics. The difference in the abrasion wear behavior of the coatings must be interpreted in terms of the interaction between the slurry and the constituents of the microstructure.

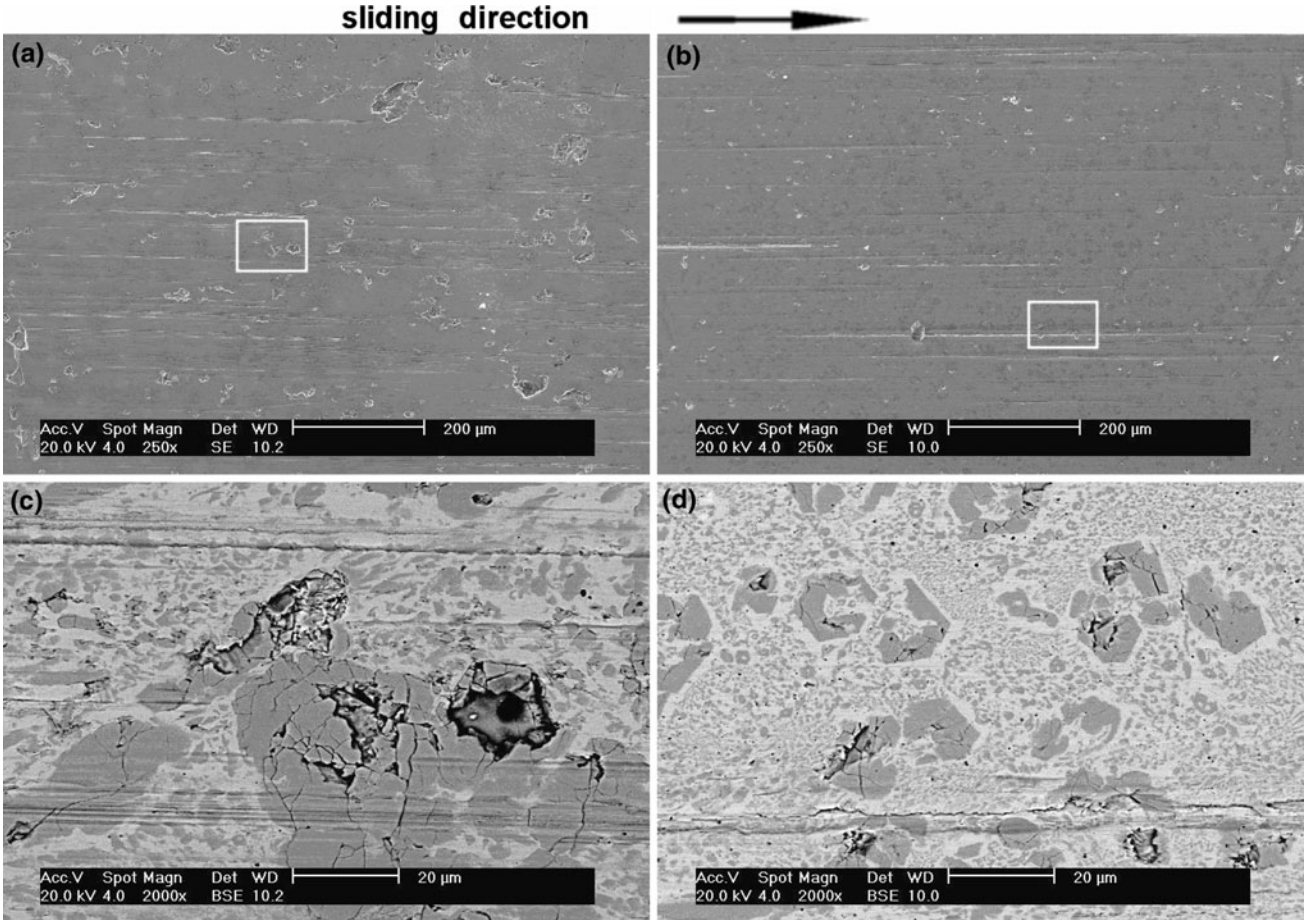

Fig. 8 Low magnification SEM plan view images of the worn surfaces of SMAW coatings in contact with slurry and bagasse board at 150 N load (a) general view of W1, SE, (b) general view of W2, SE, (c) detailed view of the rectangular section of W1, BSE, and (d) detailed view of the rectangular section of W2, BSE

4.1 Wear in the Slurries

It is clear from the SEM micrographs that most of the mass losses in the SMAW coatings occur in the fractured carbides whereas in the arc-sprayed coating, most of the mass losses occur in the main part of the wear scar. From the micrographs, it is reasonable to suggest that wear progresses by several mechanisms, mainly, microploughing, microcutting, microfatigue, and microcracking (Ref 15-17).

In the arc-sprayed coating, microploughing is the dominant mode as the material has been plastically deformed and, after repeated cycles, the displaced particles are broken off as a result of microfatigue. In the case of the SMAW coatings, microcracking, which occurs from induced stress concentration and internal faults within the carbides, appears to be the principal wear mechanism. Consequently, wear particles are detached due to crack propagation from repeated cycles. With increasing hardness, microcracking can cause drastic reduction in wear resistance and this can account for the lower wear resistance of the SMAW coatings when compared with the arc-sprayed coating. Given that microploughing involves little loss of material and with the resultant increase in hardness from strain hardening, it is reasonable to assume the arc-sprayed coating will show better wear resistant than materials undergoing wear by fracture. Since fracture was extensive in only the primary carbides, there needs to be a compromise between the size of the primary carbides and their capacity to optimize wear. It is also noticeable that the cracks in the carbides have been arrested by the austenite within the eutectic, delaying the loss of material from the surface. The matrix therefore provided two roles (1) minimizing wear by slowing the fracture of carbides and (2) supporting the carbides and allowing them to withstand greater loads.

It is imperative to recognize that the limits of experimental errors (approximately 15% in this study) can account for the measured difference in abrasive wear of the SMAW coatings in the sugarcane juice slurry. Conversely, if the measured values reflect the true behavior of the SMAW coatings, important factors that contribute to the difference in wear resistance are hardness, CVF and morphology of the carbides. Hardness, as demonstrated by previous investigators (Ref 13, 18) and reinforced in this study, is not always a reliable indicator of the abrasive wear performance of a material, particularly when comparing materials of high hardness as attained in this study. This is important especially in the case of coatings that have high CVF since the abrasion resistance may not markedly improve beyond ~35% CVF (Ref 13). Both SMAW coatings have CVFs that far exceed 35%; thus, the CVF cannot be considered the primary reason for the difference. Consideration for the better wear resistant of W2 may be attributed to its larger size primary M_7C_3 carbides, which is consistent with the

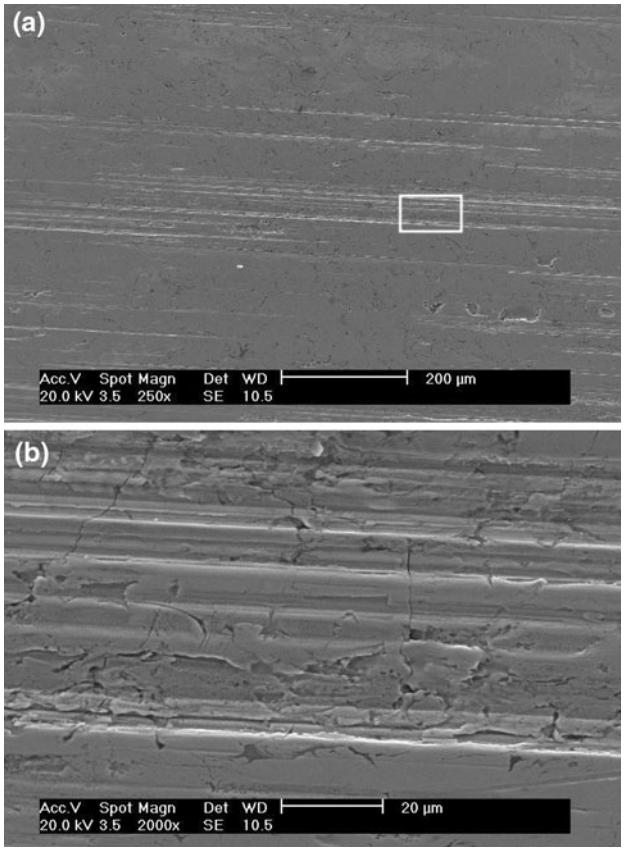

Fig. 9 Low magnification SEM plan view images of the worn surfaces of the arc-sprayed coating in contact with slurry and bagasse board at 150 N showing (a) general view and (b) magnified view of the rectangular section of (a)

findings reported by Zum Gahr and Eldis (Ref 19) who showed that coarser carbide morphology resulted in greater wear resistance than the finer carbide morphology, even though the hardness of the former was lower than the latter. The larger carbide areas in W2 were more able to withstand larger bending loads (tangential force) and more cycles to fatigue failure by crack propagation, which resulted in lower material loss.

With the introduction of glycerol at the highest load investigated, both SMAW coatings exhibited marked reduction in mass loss with identical wear resistance at the end of the test. Furthermore, in glycerol, the wear resistance of the SMAW coatings is similar to the wear resistance of the arc-sprayed coating, which exhibited no measurable change in mass loss when compared with the sugarcane juice slurry. It is quite clear that the wear resistance of the arc-sprayed coating is unaffected by the different slurries, whereas the wear resistance of the SMAW coatings depends on the type of slurry. Thus, the underlying difference in wear behavior of the coatings is inherent in their corrosion resistance characteristics.

4.2 Effect of Corrosion

The Pourbaix diagram (Ref 20) for the Fe-H_2O system can be used to estimate the corrosion behavior of the iron-based coatings, and it can be seen that the coatings are not immune in aqueous solutions. In acidic solutions containing dissolved oxygen, the overall anodic and cathodic reactions are $2Fe + O_2 + 4H_2O \rightarrow Fe(OH)_2$. Thus, as the iron constituent

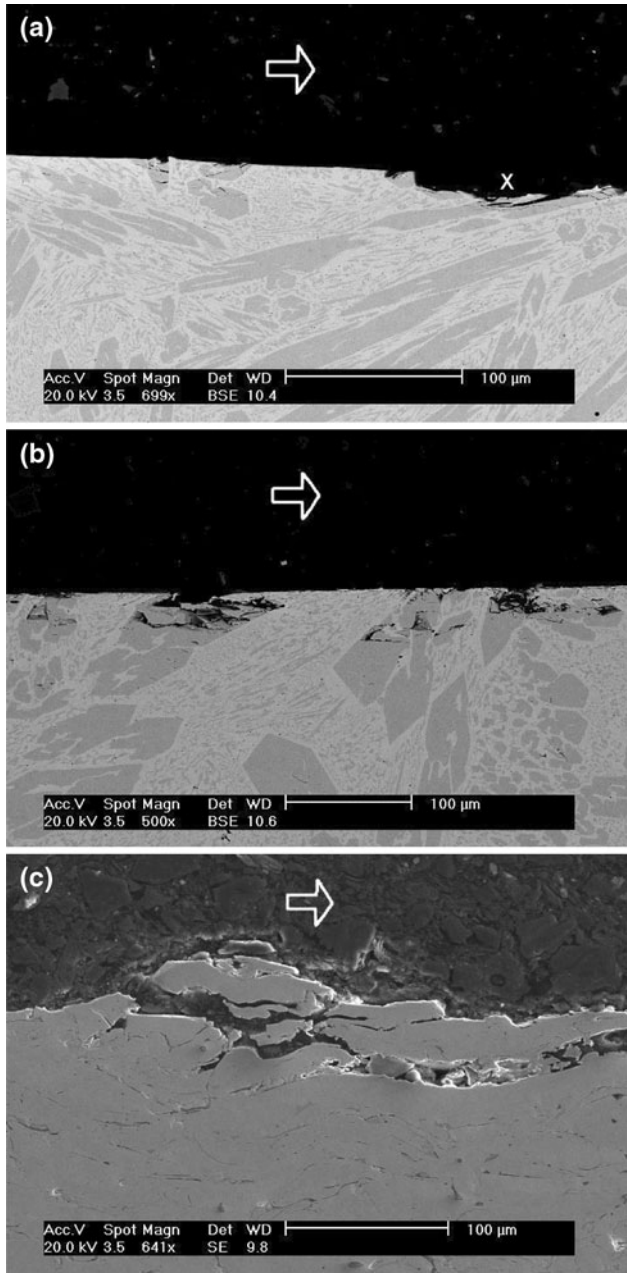

Fig. 10 Low magnification SEM images of the cross section of the coatings showing the subsurface zone following the wear test (a) W1, BSE, (b) W2, BSE, and (c) S1, SE. The arrow indicates the sliding direction

in the SMAW coatings is dissolved in the sugarcane juice, fresh carbide surfaces are exposed to the abrasives. Under the appropriate environment, salts of weak acids can provide the conditions for dissolved oxygen to form a passive oxide layer on the metal surface (Ref 21). However, under abrasion, the continued removal of the scale would accelerate the corrosion rate.

Fe-Cr alloys containing $>12\%$ Cr (Ref 22, 23) generally form an adherent Cr_2O_3 film which reduces both corrosion of the alloy and the cutting efficiency of the abrasives. However, because of the formation of a high volume fraction of M_7C_3 carbides, regions of W1 and W2 matrices are depleted of chromium. The chromium content in these regions falls below

the level needed to sustain the oxide film with subsequent vulnerability to corrosion. Indeed, the observation of such chromium-free zones around the vicinity of the primary carbides has been confirmed (Ref 22), and the influence of preferential dissolution is accentuated by the small area ratio of the anodic (matrix)/cathodic (carbide) cell. Therefore, the corrosion (in the sugarcane juice) induces additional degradation of the surface of the SMAW coatings with subsequent decrease in wear resistance when compared with glycerol.

In contrast to the SMAW coatings, the arc-sprayed coating, which had very high chromium but negligible carbon, was able to form an effective oxide layer that neutralized the effect of the sugarcane juice. This suggests that a significant amount of chromium was in solid solution form to facilitate the formation of the oxide film. Consequently, S1 effectively resisted the corrosive effect of the sugarcane juice. It is worth noting that the hardness of Cr_2O_3 is higher than the hardness of S1; thus, its presence provides additional protection from the action of the abrasives. Hence, the slight decreased observed in steady-state wear in the sugarcane juice can be accepted.

4.3 Interaction of Abrasion and Corrosion

It is generally recognized that the loss of material from the interaction of abrasion and corrosion can be defined as:

$$V = V_w + V_c + \Delta V, \quad \text{(Eq 3)}$$

where V is the total loss of material, V_w and V_c are direct losses from abrasion and corrosion, respectively, and ΔV is the synergistic amount of corrosion and abrasion (Ref 24). Assuming the corrosive and abrasive wear act independently, Ferrer et al. (Ref 25) used the factor R to assess the total synergistic effect, which is expressed as:

$$R = \frac{\Delta V}{V}, \quad \text{(Eq 4)}$$

where ΔV is the simple mass difference between the weight losses measured under abrasion-corrosion, V_{ac}, and those measured under pure abrasion, V_a, conditions, i.e.,

$$R = \frac{V_{ac} - V_a}{V_{ac}} \quad \text{(Eq 5)}$$

At a load of 150 N, the total synergistic effect of abrasion and corrosion at steady-state wear is 0.59 and 0.53 for W1 and W2, respectively, whereas R is negligible for S1. Since the surfaces of the coatings had similar roughness values after corrosion-abrasion, the overall synergism is due to the activation of electrochemical action. Therefore, within the limits of experimental error, the sugarcane juice had a detrimental effect on the SMAW coatings but not on the arc-sprayed coating.

5. Conclusion

The present study compares the abrasion-corrosion resistance of high Fe-Cr-based SMAW and electric arc-sprayed coatings in sugarcane juice and glycerol abrasive slurries. The following conclusions are drawn:

1. The abrasion-corrosion of electric arc sprayed Fe-Cr-based coating is superior to SMAW high Fe-Cr-C coatings in slurry of sand and sugarcane juice. This is principally due to the superior corrosion resistant of the arc-sprayed coating on account of it having higher amount chromium content in solid form in the matrix.
2. The effect of corrosion makes a large contribution to the lower wear resistance of the SMAW coatings owing to the depletion of chromium in the matrix from the growth of the primary carbides. In the absence of a corrosive medium, the wear resistance of the SMAW coatings is comparable to the arc-sprayed coating.
3. Microcracking of the primary carbides by fatigue with the eventual spallation of flakes of carbides is the dominant wear mechanism in the SMAW coatings. Owing to the good bonding between the austenite and the carbides, the austenite provides some measure of protection by arresting the cracks and minimizing carbide pullout. In the case of the arc-sprayed coating, microploughing is the principal mechanism of abrasive wear. As a consequence of fatigue from repeated ploughing, microcracking of the splats occurs with the eventual loss of material.

References

1. N. Maier, The Cumulative Benefits of Surface Treatment of Rolls, *Sugar Azucar*, 1981, **76**, p 60–65
2. J.L. Fluckiger, New Alternatives for the Reclamation and Coating of Mill Rolls, *Sugar Azucar*, 1991, **86**, p 16–17, 20–22
3. T.S. Falkenhagen, Mill Rollers and Abrasion Resistant Surface Coatings for Mill Rollers, Australian Patent Office, No 707580, 1999
4. H.N. Farmer, Surfacing II: Weld Overlays That Resist Corrosion, *Weld. Des. Fabr.*, 1976, p 56–59
5. R. Menon, New Developments in Hardfacing Alloys, *Weld. J.*, 1996, **75**, p 43–49
6. I.E. French and D. Klanjscek, Development of New Flux-Cored Electrodes for Arcing of Sugar Mill Roller Shells, *Proc. 27th Natl. Conf. Australia Weld. Inst.*, Vol 27, 1979, p 29–37
7. M.L. Ted Guo, C.-H. Chiang, and C.Y.A. Tsao, Microstructure and Wear Behavior of Spray-Formed and Conventionally Cast Rolls of 18Cr-2.5Mo-Fe Alloy, *Mater. Sci. Eng.*, 2002, **A326**, p 1–10
8. B.Q. Wang and M.W. Seitz, Comparison in Erosion Behavior of Iron-Base Coatings Sprayed by Three Different Arc-Spray Processes, *Wear*, 2001, **250**, p 755–761
9. T.T. Matsuo, C.S. Kiminami, W.J. Botta Fo, and C. Bolfarini, Sliding Wear of Spray-Formed High-Chromium White Cast Iron Alloys, *Wear*, 2005, **259**, p 445–452
10. V.E. Buchanan, D.G. McCartney, and P.H. Shipway, A Comparison of the Abrasive Wear Behaviour of Iron-Chromium Based Hardfaced Coatings Deposited by SMAW and Electric Arc Spraying, *Wear*, 2008, **264**, p 542–549
11. E.E. Underwood. Quantitative Metallography, *Metals Handbook*, 9th ed., Vol 9, Metallography and Structures, American Society for Metals, Metals Park, OH, 1985, p 123–134
12. E. Rabinowicz, *Friction and Wear of Materials*, 2nd ed., John Wiley and Sons, Inc, New York, 1995
13. S. Chatterjee and T.K. Pal, Wear Behaviour of Hardfacing Deposits on Cast Iron, *Wear*, 2003, **255**, p 417–425
14. O.N. Dogan, G. Laird, II, and J.A. Hawk, Abrasion Resistance of the Columnar Zone in High Cr White Cast Irons, *Wear*, 1995, **181–183**, p 342–349
15. K. Kato, Micro-Mechanisms of Wear—Wear Modes, *Wear*, 1992, **153**, p 277–295
16. K. Kato, Abrasive Wear of Metals, *Tribol. Int.*, 1997, **30**, p 333–338
17. K.-H. Zum Gahr, Wear by Hard Particles, *Tribol. Int.*, 1998, **31**, p 587–596
18. C.P. Cookson, Hardness [versus] Wear Resistance, *Surf. J.*, 1982, **13**, p 32–34
19. K.-H. Zum Gahr and G.T. Eldis, Abrasive Wear of White Cast Irons, *Wear*, 1980, **64**, p 175–194

20. M. Pourbaix, *Atlas of Electrochemical Equilibria in Aqueous Solutions*, Pergamon Press, London, 1966, p 312–313
21. G. Reinhard, M. Radtke, and U. Ramelt, On the Role of the Salts of Weak Acids in the Chemical Passivation of Iron and Steel in Aqueous Solutions, *Corros. Sci.*, 1992, **33**, p 307–313
22. L.E. Svensson, B. Gretoft, B. Ulander, and H.K.D.H. Bhadeshia, Fe-Cr-C Hardfacing Alloys for High-Temperature Applications, *J. Mater. Sci.*, 1986, **21**, p 1015–1019
23. T.M. Devine and B.J. Drummond, Use of Accelerated Intergranular Corrosion Tests and Pitting Corrosion Tests to Detect Sensitisation and Susceptibility to Intergranular Stress Corrosion Cracking in High Temperature Water of Duplex 308 Stainless Steel, *Corrosion*, 1981, **37**, p 104–115
24. T.C. Zhang, X.X. Jiang, S.Z. Li, and X.C. Lu, A Quantitative Estimation of the Synergy Between Corrosion and Abrasion, *Corros. Sci.*, 1994, **36**, p 1953–1962
25. F. Ferrer, H. Idrissi, H. Mazille, P. Fleischmann, and P. Labeeuw, A Study of Abrasion-Corrosion of AISI, 304L Stainless Steel in Saline Solution Using Acoustic Emission Technique, *NDT&E Int.*, 2000, **33**, p 363–371